京都大学防災研究所年報 第 63 号 B
DPRI Annuals, No. 63 B, 2020

High Thermal and Interaction with Convective Cloud Based from Boundary Layer Radar, Himawari-8 and Time Lapse Camera Observation (Case Study: 11 September 2018)

Ginaldi Ari NUGROHO(1), Kosei YAMAGUCHI, Eiichi NAKAKITA, Masayuki YAMAMOTO(2) and Seiji KAWAMURA(2)

(1) Graduate School of Engineering, Kyoto University, Kyoto, Japan..
(2) National Institute of Information and Communications Technology, Tokyo, Japan

Synopsis

Multiple observation to observe cloud microphysics are conducted in one of location in Kobe urban area of Japan. From Boundary Layer Radar observation capture a high thermal with its updraft properties with its height is already reaching above boundary layer height. In this period of high thermal, temperature observation from two nearest AWS showed increase of temperature value. Himawari-8 satellite and Time lapse camera capture convective cumulus cloud moving towards the thermal location in the same period. In order to analyze whether there is any effect of this high thermal towards the cumulus cloud, wavelet coherency is used. The result showed that the higher part of the thermal has the same pattern (in-phase) with the cloud albedo. High thermal seems to affect the cloud condition based on the cloud image especially in the period where the thermal reach its maximum updraft value.

Keywords: Thermal, Cumulus cloud, Updraft

1. Introduction

Column of rising air that move from surface into the atmosphere is called thermal. Thermal plumes that extended into the height of boundary layer have a important role in the mixed layer condition (Rio and Hourdin, 2008).

Urban heat island to some extent has an influence on thermal activity. There is a research that study the relationship of cloud-to ground (CG) flash density with surface temperature in urban area (Naccarato et al, 2003). Yamaguchi et al (2018) is study the thermal that break into atmosphere boundary layer in urban city.

This study will focus on case study of high thermal plume that observed by BLR in kobe urban area of Japan. The objective is to analyze whether there is an effect of this high thermal with the cloud condition that observed above the BLR site. Several other observation data are also included to support the analysis. The scope of this study is microscale with spatial area less than 500x500 meter with high temporal scale in order to be able to capture high transition of thermal and cloud condition.

2. Data and Methodology

In this study, four observation data are included for the analysis. Four datasets are from Boundary Layer Radar (BLR), Himawari-8 satellite, Time Lapse Camera, and AMeDAS JMA. Several methods are also used for processing the dataset, with one of its method is wavelet for analysis the comparison between high thermal and cloud.

2.1 Vertical velocity Boundary Layer Radar

BLR instrument is located in urban area of Kobe, Japan. These BLR is an advanced system since it equipped with range imaging (RIM) and oversampling (OS) (M. K. Yamamoto et al., 2014) technique to increase the vertical resolution and resolve perturbations of vertical wind less than 100 meter. In order to prevent clutter contamination near the ground, this BLR also equipped with adaptive clutter suppression (ACS) (M.K. Yamamoto et al., 2017).

Higher performance in temporal resolution of 8 seconds is also the advantage of this advanced BLR compare with other commercial BLR or wind profile radar available that is usually 40 – 60 second (Angevine et al., 1994; Hashiguchi et al., 1995; Ishihara et al., 2006).

Since this rapid data of BLR will be compared with the Himawari albedo satellite data, it is essential to synchronized between these two data. A moving average was performed for BLR data without reducing the characteristic of the original data. A moving average with a bin range of 95 was applied to BLR dataset and resulted a sampling period of 2.5 min (152 sec).

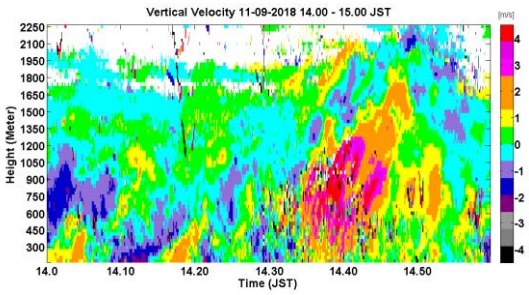

Fig. 1 BLR vertical velocity in 11 September 2018

2.2 Cloud Albedo - Himawari-8

Himawari-8 satellite data is used for verification of the cloud condition around BLR location. Himawari-8 satellite have three temporal and spatial resolution of 0.5, 2, 2.5 minutes and 0.5, 1, 2 km respectively. For cloud indicator which is the cloud albedo, data from visible band 03 of the Himawari-8 satellite are used. Figure 2 is the example of the cloud albedo data

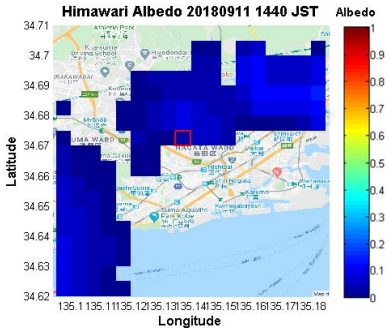

Fig 2 Cloud Albedo from Himawari-8. Red square represents the BLR location.

This band with 0.64 μm wavelength spectrum gave a large reflectance and small absorption value for clouds object compared to surface (Shang et al., 2017) . This data have 0.5 km spatial resolution but only 2.5 minutes of temporal resolution. In these studies, we only collect the data that have similar coordinate with the BLR site.

2.3 Cloud Image - Time Lapse Camera

In order to gain more high resolution of the cloud, we utilize time lapse camera. Time lapse camera is installed in the same location of the BLR and also synchronized in time using time reference from NICT website (https://www.nict.go.jp/JST/JST5_E.html).

Time lapse camera have a capturing rate of 5 frame per second which means we got 1 image in every 5 seconds. But in real situation there are several images that needs more than 5 second. This image than converted into grayscale camera for later comparison with BLR data. Quality check of the image is applied before the image dataset are used for processing.

2.4 AMeDAS JMA Surface Observation

Automated Meteorological Data Acquisition System (AMeDAS) is a network of Automatic Weather Stations (AWS) run provided by JMA for atmosphere observation of several parameter (temperature, relative humidity, precipitation, wind direction, and wind speed) with high temporal and spatial resolution. There are two AWS location that located in kobe area (Location 1= 34°41.8'N, 135°12.7'E, Location 2= 34°37.9'N, 135°13.4'E). The distance between this two AWS with BLR site is 7 to 8 km.

2.5 Wavelet Transform Coherency

In order to find whether there is a relation between vertical velocity thermal and cloud albedo, or also vertical velocity from thermal and cloud image camera, we used Wavelet Transform Coherency (WTC) method. WTC method is used in order to analyze the connection between two process based on the time intervals and frequency occurrence (Ng, Eric and Chan, 2012).

WTC is a technique used to find relationship from two dataset based on changes of frequency scale and time intervals (Ng, Eric and Chan, 2012). WTC not only give a quantitative correlation but also give the phase angle between two variables (cloud albedo and vertical velocity).

These two variable are then normalized, calculate the wavelet power spectrum (Wx , Wy), calculate the cross wavelet (Wxy), and calculate wavelet coherence (R^2(s) and ϕ) as in eq. (1) and (2) respectively. The algorithm of this process are based from the work by Grinsted et al (2004) that have been modified.

$$R_n^2(s) = \frac{\left[W_n^{xy}(s)\right]^2}{\left[W_n^x(s)\right]^2\left[W_n^y(s)\right]^2} \quad (1)$$

$$\phi = \tan^{-1}\frac{imaginary(W^{xy})}{real(W^{xy})} \quad (2)$$

Before calculate WTC, first we need to calculate the wavelet power spectrum using Continuous Wavelet Transform (CWT) method. CWT is used because of its ability to extracting certain characteristic (Wiebe 2011). In these studies, CWT is used to identified the updraft that correspond with thermal structure based on the vertical velocity data from BLR. In these studied, the CWT application are based on algorithm developed by Torrence and Campo (1998) with main equation is in equation 3.

$$W_n(s) = \sum_{n'=0}^{N-1} X_{n'} \Psi^* \left[\frac{(n'-n)\delta t}{s}\right] \quad (3)$$

where Ψ* is the complex conjugate of the wavelet function based on chosen mother wavelet, s is the wavelet scale , N is the number amount of time series Xn'. To calculate the wavelet scale, we need to determine the smallest (s_0) and largest (s_j) values based on equation 4, and also number of scales used (j) based on equation 5.

$$s_j = s_0 2^{j\delta_j} \quad (4)$$

$$j = \left(log_2(N\delta t/s_0)\right)/\delta j \quad (5)$$

With this sampling period and a time period of 11 hours results δt value of 0,37. Then, using equation 2 and 3 resulted the smallest and largest scale value of 0.74 and 112, respectively. Because applying the fractional power of two, the largest scale value became 128. The number of scales used is 28 scales. Mexican Hat mother wavelet are applied in CWT with scale and time step resolution are 28 scale and 2.5 minutes respectively.

2.6 Atmospheric Boundary Layer Height

In order to found out whether the upper thermal structure penetrate the boundary layer height, we need to estimate the boundary layer height is self. The method used is based on studies by Angevine et al. (1994) that uses BLR echo power and calculate its every peak of certain period and then calculated using median to get the estimated boundary layer height.

We use this boundary layer height as a threshold to distinguish which of the updraft from thermal structure dataset that could penetrate the boundary layer height. This dataset then further analyzed by calculate its correlation with the existence of the cloud albedo from Himawari-8 data.

2.7 Vertical Velocity Variance

Variance from vertical velocity is use to estimate the fluctuating component. The decrease of vertical velocity variance is a indication of the convective boundary layer or inversion layer top or in this case is the atmospheric boundary layer height. Variance is calculated based on equation 6 (Scipion et al., 2009).

$$\sigma^2 = \overline{w'w'} \quad (6)$$

3. Result and Discussion

Meteorological factor is inspected in three days between 9 – 11 September 2018 from two nearest AMeDAS AWS. Figure 3 is the temperature observation every 10 minutes, where from 14.00 – 15.00 JST is the highest temperature (27^0 C) in 11 September 2018 and also the other 2 days before.

During this period, it is reasonable if the thermal activity is very active based on temperature observation.

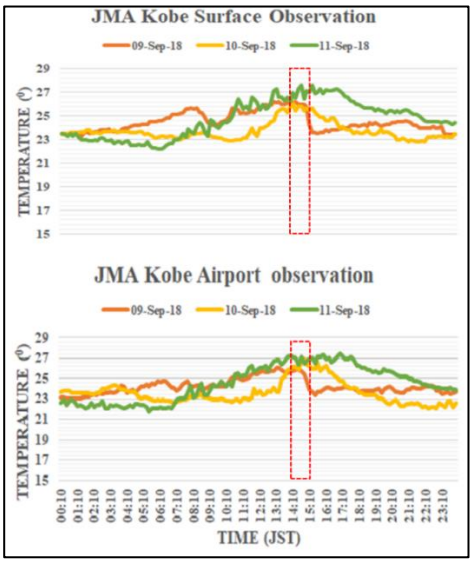

Fig. 3 Temperature observation from nearest JMA AMeDAS in Kobe area.

In figure 4, compared with the vertical velocity data from BLR in these period (14.00 – 15.00 JST) we find very strong thermal activity in 11 September 2018 compared to 10 September 2018, meanwhile 9 September 2018 there is rain occur which is why BLR cannot observe thermal activity.

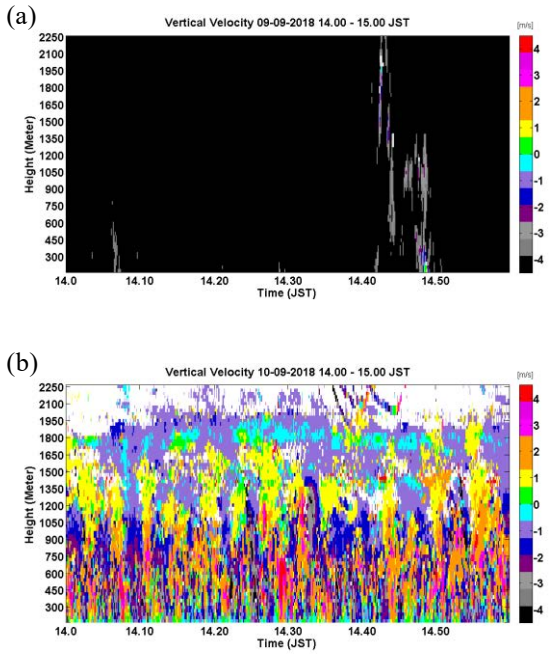

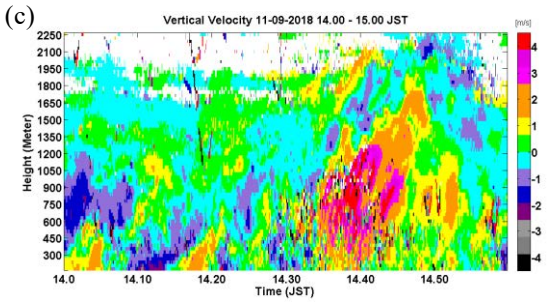

Fig. 4 Vertical velocity from BLR observation, (a) 9-9-2018, (b) 10-09-2018, (c) 11-09-2018

In this study, we would like to observe this high thermal in 11 September 2018. From advanced BLR observation, this high thermal is captured with maximum updraft value more than 5 m/s. The thermal reaching up to 1.7 km height with the period occur around 10 minutes.

First thing that need to achieve in this study is to calculate the boundary layer height in order to find that whether the thermal have penetrated the boundary layer or not. Figure 5a. is the estimated boundary layer height based on Angevine method (Angevine et al., 1994) where vertical velocity from BLR data are overlay with the black box-line shape which represent the estimated boundary layer height.

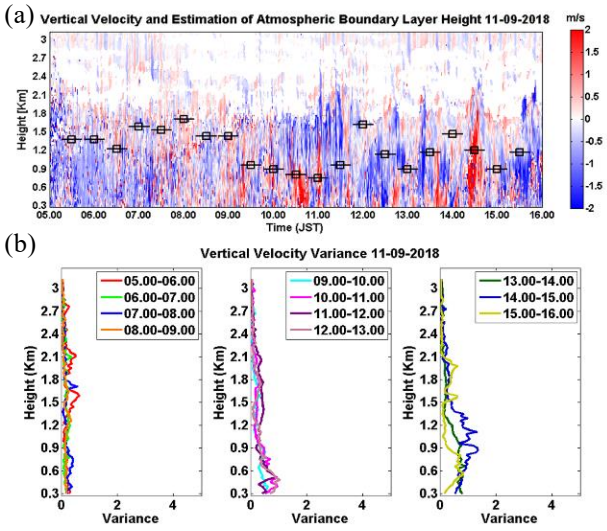

Fig. 5 Atmosphere boundary layer height, (a). Estimated boundary layer height from echo power, (b). Variance from vertical velocity.

Focused on period of high thermal which from 14.00 to 15.00 JST, the estimated boundary layer height is around 1.2-1.5 km. This estimated height is also supported from the variance of the vertical

velocity profile (Figure 5b) where the minimum variance value in this period are located in 1.5 km height. The maximum height of the thermal is 1.7 km so it means that the thermal has penetrate the boundary layer height.

In order to check the influence of the thermal towards the incoming cloud, existence of cloud is first checked from cloud albedo data. Figure 6 is the time series of the cloud albedo data extracted from period 14.00 – 15.00 JST above the BLR site. From this result, the maximum albedo value is occurred in 14.40 JST. In order to analyze the relation of this cloud albedo time series with the vertical velocity activity, WTC are then applied.

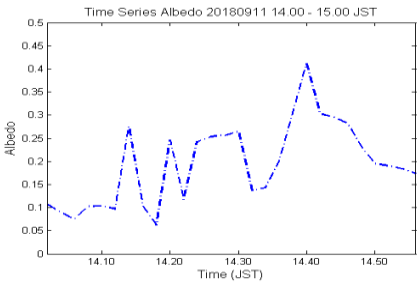

Fig. 6 Time series of cloud albedo above BLR site.

Before applied the WTC, both dataset (cloud albedo and vertical velocity) are normalized in order to have the same unit with these two datasets. Figure 7 is the WTC result with different height of vertical velocity data. Two graphs on the left, represent the normalized-time series of cloud albedo and vertical velocity (in variated height). The other represent the wavelet coherency result.

Colored data in the wavelet coherency represent the correlation level (high = 1, low = 0). Black line area represented the 95% of confidence level with coherency value from 0.7 – 1 as threshold. Arrow represent the phase correlation with four classification based on the arrow direction, Right arrow (in phase), left arrow (anti phase), Down arrow (vertical velocity leading cloud albedo by 90^0 or 2.5 minutes), Up arrow (cloud albedo leading vertical velocity by 90^0 or 2.5 minutes). The resume of the WTC phase coherency result is listed in table 1.

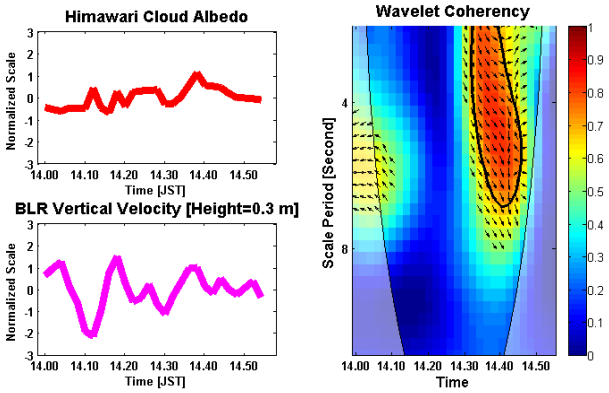

(a)

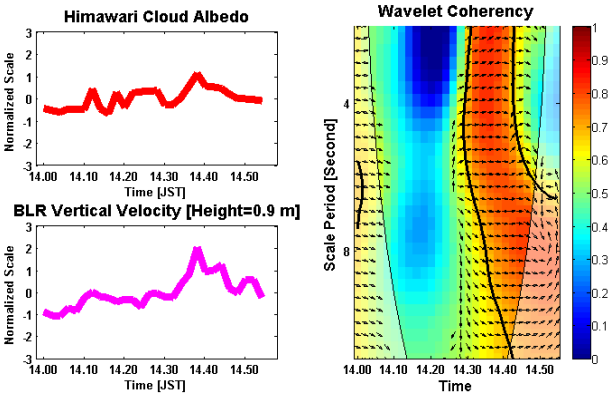

(b)

Fig. 7 WTC result, (a) 0.3 km, (b) 0.9 km.

From this result showed that from height level of 0.3 km until 0.8 km, dominant phase is down arrow (except for 0.4km which is right arrow), which means that dominantly vertical velocity is leading cloud albedo. It means that thermal is generated before cloud passed by.

Table 1. Phase Angle (vertical velocity-cloud albedo)

Height (km)	Phase Angle	Height (km)	Phase Angle
0.3	Down	1.2	Right
0.4	Right	1.3	Right
0.5	Down	1.4	Right
0.6	Down	1.5	-
0.7	Down	1.6	-
0.8	Down	1.7	-
0.9	Right	1.8	Down
1.0	-	1.9	-
1.1	Right	2.0	-

From 0.9km until 2.0km, the dominant phase correlation is right arrow (except in 1.8 km which is down arrow) which means that cloud albedo and vertical velocity pattern are in-phase cloud albedo pattern. The thermal presence in the lowest height from 0.3km until 0.8 km is not affected by the cloud existence based from the phase angle result. Meanwhile in the highest level from 0.9 km until 2.0 km, the thermal is affected by the cloud presence with the pattern are similar.

Fig. 8 Cloud Image from Time Lapse Camera 14.26 – 14.36 JST

Cloud image from time lapse camera give more high temporal resolution of cloud existence above BLR location. Figure 8 is the cloud image from 14.26 – 14.36 JST to complement the analysis. This sequence image showed the incoming cloud above BLR site.

Average time series of grayscale cloud image is showed in Fig 9. In this time series showed a decrease pattern from 14.28 until 14.34 JST which also similar with the pattern of cloud albedo from Himawari-8. This probably because of the existence of stratus cloud before convective cloud passed. The increase is started after 14.34 JST – 14.36 JST that will be focused for transition phase. Unfortunately, the cloud is becoming darker after 14.36 JST and give a decrease pattern although the cloud size is become bigger and wider. The dataset from 14.34 JST – 14.36 JST are then calculated again using wavelet coherency (Figure 10) with the result are summarized in table 2.

From table 2 from 0.3 km - 0.7 km the phase is the same with previous WTC result (vertical velocity-Cloud albedo), but after that the phase is variated. This result showed that in the lower part, the thermal is generated first before the cloud appear.

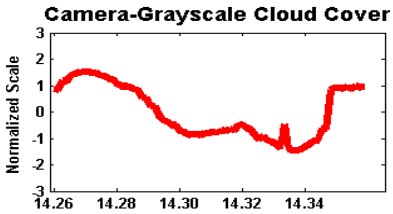

Fig. 9 Time series Grayscale Cloud Image

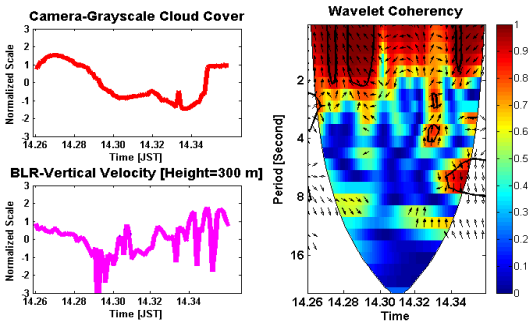

(a)

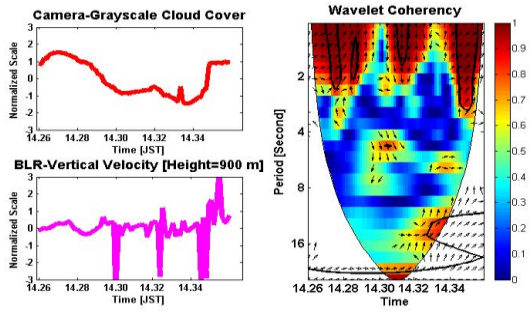

(b)

Fig. 10 WTC vertical velocity-cloud image, (a) 0.3 km, (b) 0.9 km.

Table 2. Phase Angle (Vertical velocity - Grayscale cloud image)

Height (km)	Phase Angle	Height (km)	Phase Angle
0.3	Down	1.2	Right
0.4	Right	1.3	Down
0.5	Down	1.4	-
0.6	Down	1.5	Up
0.7	-	1.6	Right
0.8	Down	1.7	Down
0.9	Right	1.8	-
1.0	Up	1.9	Left
1.1	-	2.0	-

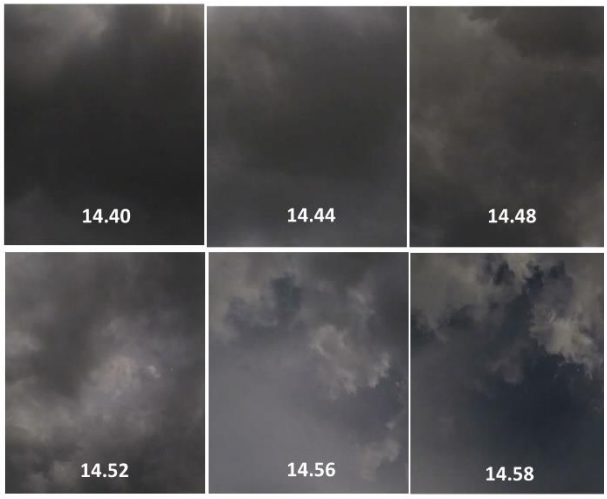

Fig. 11 Cloud Image from Time Lapse Camera 14.40 – 14.58 JST

Two WTC result showed the relationship of the high thermal with the convective cloud that passed above BLR site. Lower part of the thermal is not affected the cloud, meanwhile the upper part is having the same pattern (in-phase) with the cloud existence. The upper part of the thermal seems to affected the cloud.

The effect of the upper thermal towards the convective cloud is probably can be described by the cloud image after 14.36 JST (Figure 11). The cloud is become darker in 14.40 JST and showed some rotation from the image sequence in 14.44 JST and dissipated in 14.58 JST. This result showed that high thermal can affect the convective cloud condition although it seems not increasing the convective activity of the cloud towards a precipitation.

4. Conclusion

High thermal activity is occurred in 11 September 2018 from 14.30 until 14.50 JST in Kobe urban area of Japan. Based from two nearest available AWS data in this period, maximum temperature is observed in the range of 27^0C. Detailed high thermal activity is observed by advanced BLR. The high thermal is having a maximum updraft value of more than 5 m/s with the thermal reaching up to 1.7 km height. This height is already surpassing the atmospheric boundary layer height which is estimated to be in 1.5 km height level based on Angevine method and vertical velocity variance. From Himawari-8 satellite data showed that there are convective cloud passing by the thermal with maximum albedo at 14.40 JST. Based from time lapse camera showed that the cloud is right above the BLR site at 14.36 JST. Using wavelet coherency showed that the higher part of the thermal is affected by cloud existence. During maximum thermal value in 14.40 JST, the cloud image is become darker and showed some rotation in 14.44 JST. This result showed that high thermal can affect the convective cloud condition although it seems not increasing the convective activity of the cloud towards a precipitation cloud.

Acknowledgements

This work was supported by KAKENHI, 15H05765, 20H02258, 16K12861.

References

Angevine, W. M., White, A. B., and Avery, S. K. (1994): Boundary-layer depth and entrainment zone characterization with a boundary-layer profiler, Boundary-Layer Meteorology, 68(4), 375-385.

Erick K.W.Ng and Johny C.L.Chan. (2012): Geophysical Application of Partial Wavelet Coherence and Multiple Wavelet Coherence, Journal of Atmospheric and Oceanic Technology, Vol 29, pp 1845-1853.

Naccarato, K. P., Pinto Jr, O., and Pinto, I. R. C. A. (2003): Evidence of thermal and aerosol effects on the cloud‐to‐ground lightning density and polarity over large urban areas of Southeastern Brazil, Geophysical Research Letters, 30(13).

Rio, C., and Hourdin, F. (2008): A thermal plume model for the convective boundary layer: Representation of cumulus clouds, Journal of the atmospheric sciences, 65(2), 407-425.

Scipión, D., Palmer, R., Chilson, P., Fedorovich, E., and Botnick, A. (2009): Retrieval of convective boundary layer wind field statistics from radar profiler measurements in conjunction with large eddy simulation, Meteorologische Zeitschrift, 18(2), 175-187.

Shang, H., Chen, L., Letu, H., Zhao, M., Li, S., and

Bao, S. (2017): Development of a daytime cloud and haze detection algorithm for Himawari‐8 satellite measurements over central and eastern China, Journal of Geophysical Research: Atmospheres, 122(6), 3528-3543.

Torrence. C and G.P.Campo. (1998): A Practical Guide to Wavelet Analysis. Bulletin of the American Meteorological Society, Vol.79, 61-78.

Wiebe, A., Sturman, A., and McGowan, H. (2011): Wavelet analysis of atmospheric turbulence over a coral reef flat, Journal of Atmospheric and Oceanic Technology, 28(5), 698-708.

Yamaguchi K, Konishi D, Tsuchihasi T, Nakakita E, Yamamoto M, Kawamura S, Amagai J, Sugitani S, Ohigashi T, and Ogawa M. (2018): Discovery of Thermals Breaking through Atmospheric boundary Layer by Urban Meteorological Model Based on Large Eddy Simulation and Boundary Layer Radar, DPRI Annuals, No 61 B, 2018.

Yamamoto, Masayuki K., Toshiyuki Fujita, Noor Hafizah Binti Abdul Aziz, Tong Gan, Hiroyuki Hashiguchi, Tian-You Yu, and Mamoru Yamamoto, (2014): Development of a digital receiver for range imaging atmospheric radar, Journal of Atmospheric and Solar-Terrestrial Physics ,118, 35-44.

Yamamoto, Masayuki K., Seiji Kawamura, and Koji Nishimura. (2017): Facility implementation of adaptive clutter suppression to an existing wind profiler radar: First result. IEICE Communications Express ,6(9), 513-518.

(Received August 31, 2020)